Bridging steady-state and stick-slip fracture propagation in glassy polymers

Yannick Nziakou, Guillaume Fischer, Matthieu George, Bruno Bresson, Mathilde Tiennot, Stéphane Roux, Jean-Louis Halary, Matteo Ciccotti

Bridging steady-state and stick-slip fracture propagation in glassy polymers

Yannick Nziakou,[a] Matthieu George,[b] Guillaume Fisher,[a] Bruno Bresson,[a] Mathilde Tiennot,[a] Stephane Roux,[c] Jean-Louis Halary,[a] and Matteo Ciccotti [a*]

Received XX, Accepted XX
First published on the web XX
DOI: XX/XX

Both an experimental and a theoretical investigation of the fracture propagation mechanisms acting at the process zone scale in glassy polymers are presented. The main aim is to establish a common modeling for different kinds of glassy polymers presenting either steady-state fracture propagation or stick-slip fracture propagation or both, depending on loading conditions and sample shape. On the experimental point of view, new insights are provided by in-situ AFM measurements of the viscoplastic strain fields acting within the micrometric process zone in a brittle epoxy resin, which highlight an extremely slow unexpected steady-state regime with finite plastic strains of about 30% around a blunt crack tip, and accompanied by propagating shear lips. On the theoretical point of view, we apply to glassy polymers some recently developed models for describing soft dissipative fracture that are pertinent with the observed finite strains. We propose a unified modeling of the fracture energy for both the steady-state and stick-slip fracture propagation based on the evaluation of the energy dissipation density at a characteristic strain rate induced in the process zone by the competition between the crack propagation velocity and the macroscopic sample loading rate.

1 Introduction

Fracture propagation in glassy polymers has been widely studied in the '70s and '80 [1–3]. Although glassy polymers share very similar linear properties up to yielding, the kinetics of fracture propagation at a macroscopic scale appears to be very different depending on the structure of the macromolecular network.

For thermoplastics (such as PMMA) slow fracture propagation is a smooth process up to a maximum velocity V_{max} where an instability occurs leading to dynamic crack propagation. The fracture properties are described by a curve reporting the toughness* $K_C(V,T)$ or the fracture energy $\Gamma(V,T)$ as a function of the steady-state crack propagation velocity V and temperature T (cf. Fig. 1(top)) [1]. The quasi-static slow regime and the dynamic regime are associated to the two positive slope regimes of the $\Gamma(V)$ curve, which are separated by a hypothetic negative slope region (dashed in Fig. 1(top)) where steady-state crack propagation is unstable and can not be measured [4]. The slow quasi-static regime extends over several decades of propagation velocities and the $\Gamma(V)$ curve is dominated by viscoplastic dissipation in a crack-tip process zone of the size of tens of micrometers according to Dugdale model [5,6].†

For thermosets (such as epoxy resins) fracture propagation is affected by stick-slip dynamics [9]. A static crack will not propagate up to an initiation value $K_{start}(\dot{\delta},T)$ that is a decreasing function of the loading rate $\dot{\delta}$ applied to the sample and an increasing function of temperature. Then dynamic propagation will follow ($V \sim 100$ m/s) inducing a rapid unloading of the sample [10]. Eventually, the crack will stop for a lower value of K, called K_{stop}, which is quite insensitive to both the rate of loading and temperature [11]. Kinloch and Williams [9] have shown that the measurements of $K_{start}(\dot{\delta},T)$ for several epoxy based glassy polymers can be condensed into an elegant master curve (cf. Fig. 1(bottom)) when plotting the ratio of $K_{start}(\dot{\delta},T)/K_{stop}$ against the yield stress σ_y of the material, which is an increasing function of the strain rate $\dot{\varepsilon}$ (and thus the loading rate $\dot{\delta}$) and a decreasing function of temperature T. When increasing the loading rate (or decreasing temperature), the amplitude of the stick-slip dynamics progressively fades into a macroscopically stable brittle crack propagation regime, which is quite insensitive to both $\dot{\delta}$ and T.

In section 2 an original in-situ AFM investigation with

[a] *Laboratoire Sciences et Ingénierie de la Matière Molle (SIMM), PSL Research University, UPMC Univ Paris 06, ESPCI Paris, CNRS, 10 rue Vauquelin, 75231 Paris cedex 05, France. E-mail: matteo.ciccotti@espci.fr*
[b] *Laboratoire Charles Coulomb (L2C), UMR 5221 CNRS-Universitéde Montpellier, FR-34095, Montpellier, France.*
[c] *Université Paris-Saclay, ENS Paris-Saclay, CNRS, Laboratoire de Mécanique et Technologie (LMT), F-91190, Gif-sur-Yvette, France*

* In this manuscript we systematically refer to mode I (opening) toughness, which is the most relevant for bulk fracture propagation.

† Let us stress that the term "process zone" for the viscoplastic dissipative region is not universal. In some different community this is used to mean the intrinsic damage region [7].

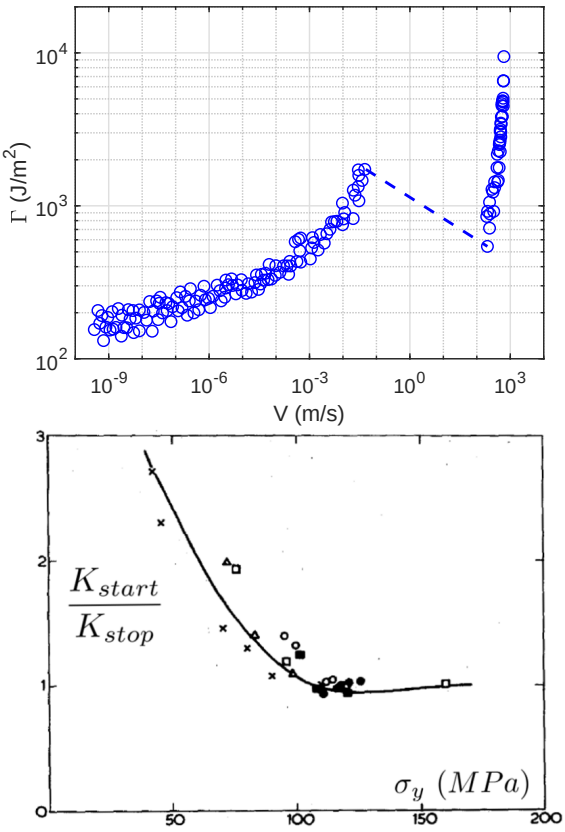

Fig. 1 (top) Steady-state crack propagation curve $\Gamma(V)$ in a typical thermoplastic glassy polymer (PMMA, data from[5,8]). (bottom) Master curve for the stick-slip crack propagation for several thermosets: K_{start}/K_{stop} as a function of the yield stress σ_y, which is an increasing function of the loading rate $\dot{\delta}$ and a decreasing function of temperature (from[9]).

nanometric resolution is presented. It shows for the first time that for brittle thermosets like epoxy resin, a steady-state slow crack propagation behavior can be observed in the same way as in thermoplastics, but with velocities limited to less than one nm/s. Moreover, it allows unprecedented visualization and real-time measurement of the strain fields at the scale of the micrometric process zone during crack propagation.

In section 3 a theoretical modeling inspired by both these novel observations and by recent developments on the fracture of soft dissipative materials[12] is introduced. The aim is to show that the steady-state crack propagation curve $K_C(V)$ and the characteristic stick-slip curve $K_{start}(\dot{\delta})$ are two complementary facets of a unified crack propagation physics for all glassy polymers, in an analog way to what is observed in the peeling of adhesive tapes[4].

In section 4 the unified model is evaluated in light of our experimental measurements as well as complementary data and investigations from the literature on glassy polymers leading to a better physical interpretation of the basic ingredients of the model, before the main conclusions are summarized in section 5.

2 In-situ AFM investigation of slow crack growth

2.1 Materials

As a model thermoset polymer the epoxy-amine DGEBA-IPD (DiGlycidyl Ether of Bisphenol A, cured with a stoichiometric ratio of IsoPhorone Diamine, both from Sigma-Aldrich) is selected[13]. After 30 minutes stirring and degassing in a vacuum oven, the mixing was cured at 60°C for 12 h and then at 195°C for 24 h. The cured sample was allowed to slowly cool down to room temperature in order to minimize internal stresses. The set polymer is then machined into DCDC samples.

This curing process results in a very densely cross-linked chemical network, with an elevated glass transition temperature of $T_g = (167 \pm 10)$°C and a Young modulus $E = (1.9 \pm 0.2)$ GPa (both measured by DMA at 1 Hz, cf.[13]). The room temperature compressive yield stress is reported in Table 1 as a function of the applied strain rate. This was measured by uniaxial compression tests performed on cylindrical pillars of 4 mm diameter and 5 mm height lubricated by molybdenum disulfide grease as reported in Fig. 2. We can remark that the present epoxy resin does not present any appreciable post-yield softening. Although we represented the failure point for the compressed cylinders in Fig. 2, this should not be interpreted as a material parameter, since it depends both on the stress triaxiality and on the erratic failure modes of compressed cylinders.

2.2 Extension of DCDC technique to glassy polymers

The Double Cleavage Drilled Compression (DCDC) sample was initially developed by Janssen[15] to study slow fracture in silicate glasses, which possess very high values for both Young modulus $E \approx 70$ GPa and yield strength $\sigma_y \approx 10$ GPa. The sample (Fig. 3a) consists of a prism of dimensions $2L \times 2w \times 2t$ (corresponding to x, y, z directions) with a cylindrical cross hole of radius R drilled through the specimen thickness $2t$. The sample is loaded with a compressive force F, and thus

Table 1 Yield stress σ_y measured by compressive tests on cylindrical pillars as at variable strain rates (cf. Fig. 2). The values of σ_y were extracted with the method of tangents according to Ref.[14]

$\dot{\varepsilon}$ (s^{-1})	10^{-3}	10^{-2}	10^{-1}	10^{0}	10^{1}
σ_y (MPa)	108	118	125	143	152

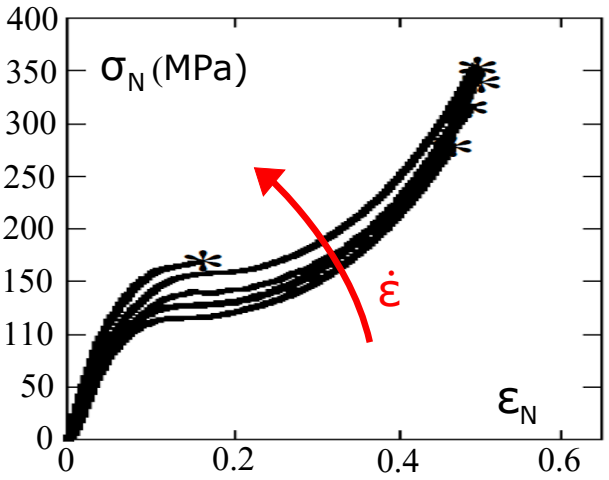

Fig. 2 Uniaxial compression testing up to failure (star symbol) of cylindrical samples of DGEBA-IPD at $T = (23 \pm 1)^{\circ}$C for increasing values of the strain rate reported in Table 1 (Figure after Ref.[13]).

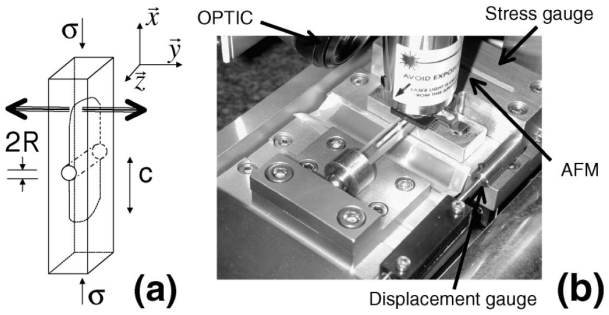

Fig. 3 Experimental setup: (a) Sketch of the DCDC geometry; (b) picture of the experiment, including the DCDC sample on a loading stage under the AFM probe.

a compressive stress $\sigma = F/4wt$ applied to the two opposite faces. This induces a tensile stress at the two poles of the central hole aligned with the sample loading direction. During the test in stiff and hard materials like glass, two symmetric cracks of length c are spontaneously nucleated at the crown of the central hole. The two cracks then propagate in opposite directions along the midplane of the sample (direction x in the $x-z$ plane), driven by the mode I opening induced at the crack tips.

In a previous paper[16], this novel technique was shown to be suitable to obtain both a successful crack initiation and well conditioned steady-state crack propagation in PMMA samples, which is a typical thermoplastic glassy polymer with a well known $K_C(V)$ curve. Glassy polymers are less stiff ($E \approx 1$ GPa) and less hard ($\sigma_y \approx 100$ MPa) than silicate glasses. Moreover, they present a slow viscoplastic relaxation at macroscopic scale. Since these materials are not brittle enough to provide a spontaneous crack initiation from the central hole, the crack initiation has to be implemented with the help of instrumented blades[17]. Sample dimensions have to be optimized in order to minimize buckling and yielding during crack propagation while preserving the small sample dimension required by *in-situ* AFM investigations (for epoxy resin this leads to $2L = 40$ mm, $2w = 8$ mm, $2t = 4$ mm and $R = 1.33$ mm). Due to the occurrence of stress relaxation, larger deformations and plastic yield, especially in the shear stress concentration region close to the central hole, the standard LEFM equations to evaluate the stress intensity factor K from linear elastic finite element modeling of DCDC sample[18] do not apply conveniently to glassy polymers[19]. An original method was developed to estimate the stress intensity factor K based on the fit of the experimental measurement of the crack opening profile $u_y(X)$ at the millimetric scale of the elastic region surrounding the process zone (far from the central hole where bulk plastic yielding can occur)[16] with the following Williams expansion[18]:

$$u_y(X) = \frac{K}{E'}\sqrt{\frac{8X}{\pi}}\left(1 + 1.319\frac{X}{w} + 0.515\left(\frac{X}{w}\right)^2\right) \quad (1)$$

where X is the distance from the crack tip, and $E' = E/(1-\nu^2)$ because plane-strain conditions are dominant in our specimen at the scale of this measurement. Since the accuracy of this technique is limited to 10%, which is comparable with the small range of variation of $K_C(V)$ for glassy polymers, this fitting procedure should be limited to set the average value of K during the test[16]. In order to obtain the complete $K_C(V)$ curve, the crack length c is considered to be essentially unchanged during slow crack propagation ($v < 10$ nm/s for AFM investigations). The measured stress relaxation $F(t)$ in the DCDC sample is thus dominated by visco-elasto-plastic creep. The recording of the measured applied force $F(t)$ could thus be used to directly obtain the relative time evolution of $K_C(t)$. This was then combined with the measurement of the crack tip velocity $V(t)$ performed by optical or atomic force microscopy. The $K_C(V)$ curve obtained for PMMA was shown to be in excellent agreement with data from the literature[5].

2.3 In-situ AFM observations in epoxy resin

Figure 4 represents a typical image that was obtained in the process zone at the crack tip in our epoxy resins (right), which immediately appears to be very different from our previous observation on PMMA thermoplastic (left), revealing the richness of information on the detailed mechanisms in action at the process zone scale.

The surface displacement in epoxy appears as a very smooth field with a clear monotonic strain concentration towards the

crack tip. This feature is very different from what was observed for PMMA, where a very extended surface necking region was associated to localized shear yielding due to low stress triaxiality near the external surface, while secondary grooves were interpreted as marks of secondary crazes originating at surface defects and propagating towards the bulk of the sample [16]. The absence of crazing in epoxies is consistent with literature and is generally attributed to the high crosslinking density [20].

By carefully handling the AFM drifts, *three weeks* of continuous in-situ AFM imaging was performed on the same location corresponding to a crack tip that reached an arrest (stick) after dynamic propagation in the pop-in phase (slip). The most striking result is that this arrested crack in a brittle epoxy indeed keeps propagating at a very low velocity, with an average of 8 pm/s, which is about an atomic step every ten seconds. This is clearly illustrated in Fig. 5, where AFM deflection error images [16] flatten out the surface topography to reveal the smallest surface defects, which act as a speckle pattern on the sample surface.

Moreover, when analyzing the full in-situ AFM image series (the movie is provided as a Supplementary Material) the crack propagation velocity is found to be very regular and to slowly decrease from 18 to 3 pm/s over three weeks, while the measured applied force concomitantly decreases from 810 to 750 N. This allows to use the AFM image series to measure the $K_C(V)$ curve in the covered velocity range. Since the crack length ($c \simeq 4.5$ mm) only increases by 15 µm during the series, the decrease of the force (at constant applied displacement) can be solely attributed to viscoplastic stress relaxation, according to the methods described in previous section. The $K_C(V)$ curves obtained for three different epoxy samples with the same procedure are reported in Fig. 6.

While the measured $K_C(V)$ curves for epoxy are quite similar in slope to what can be obtained from the data of PMMA in Fig. 1(top) (in the lower velocity domain), there is a striking difference between these two materials, since the slow fracture propagation in PMMA can be observed up to $V_{max} \simeq 1$ cm/s, [5] while in epoxy the maximum measured velocity before the dynamic instability was found here to be $V_{max} \simeq 1$ nm/s, which is 7 decades smaller. In order to measure this maximum velocity, the displacement applied to the sample was increased by steps and the load and crack propagation velocity were measured each time, up to the step where the fracture becomes dynamic and the sample suddenly breaks. This very low maximum velocity in the nm/s range, comparable to the growth rate of humain nails, can explain why such propagation was never detected before, since most investigations on fracture of epoxys were done in the '70s mainly by optical techniques [11].

In-situ topographic AFM images directly provide the out-of-plane component u_z of the crack tip displacement field,

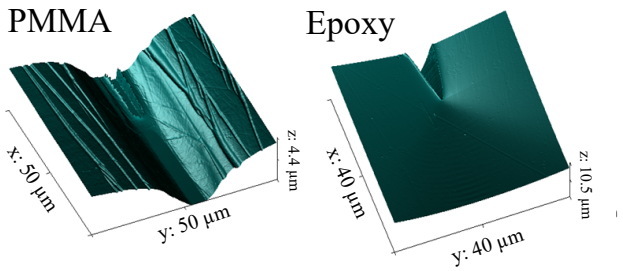

Fig. 4 3D representation of the topography of the crack tip region measured by AFM at the free surface of PMMA (left) and epoxy resin (right) samples. Left image from [16].

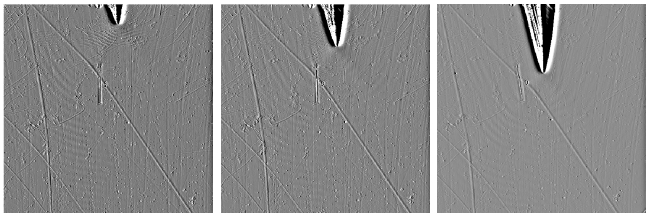

Fig. 5 2D flattened images (AFM deflection error signal) representing three successive steps of crack propagation in epoxy over three weeks. The full size of the images is 50 μm. The crack propagates in the x direction.

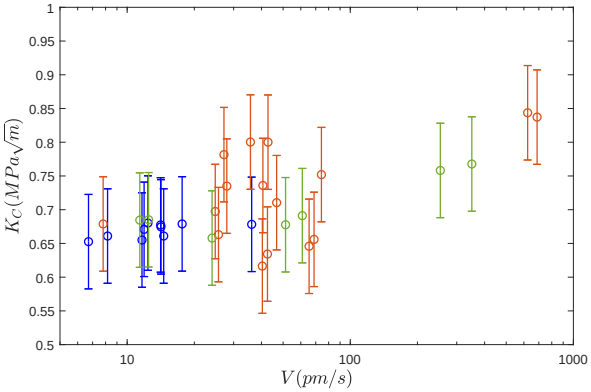

Fig. 6 Measured $K_C(V)$ curves for three different samples of the DGEBA-IPD epoxy resin.

which is much larger than surface roughness. The in-plane components (u_x, u_y) can be obtained by tracking the change of relative position of a series of surface defects that are visible in Fig. 5. In order to estimate the 2D nominal strain tensor components ε_{yy} and ε_{xx} of the sample surface, some triads of remarkable points were chosen, such that they would form two approximately orthogonal segments of gauge length $L_T \simeq 2$ µm, aligned along x and y (the details of the technique can be found in Ref [16]). The average strain components associated

to the center position x_T, y_T of the triad are thus obtained by dividing the appropriate displacement differences by the segment lengths. Fig. 7 presents the evolution of these strain components as a function of their distance from the crack tip on a couple of segments centered on the crack axis ($y_T \simeq 0$ µm). The extensional strain ε_{yy} orthogonal to the crack direction presents a significant rise starting at a distance of about 7 µm from the crack tip and then follows an approximately linear trend up to a maximum of about 30%, measured at a distance of about 2 µm from the crack tip. The longitudinal strain component ε_{xx} did not present any significant trend out of the 5% scatter that constitutes the detection limit. In light of the large values of the measured strain field and the permanent nature of both the out-of-plane and in-plane strain fields along the crack lips after the crack tip has passed, the measured crack tip fields can soundly be associated to plastic yield. It is to be emphasized that the measured strain does not correspond to the total strain, since the initial reference image is already affected by an elastic strain (which can be estimated to be of the order of the yield strain $\varepsilon_y \simeq 8\%$), which affects a region much larger than the image size and than the distance traveled by the crack[‡]. The measured values for the process zone size and the maximum plastic strain are compatible respectively with Dugdale estimation of the process zone size[6] and with the maximum strain allowed by the stretchability of the tightly cross-linked polymer network[20]. This handmade image correlation technique is thus very efficient for identifying the size of the plastic process zone and to evaluate the plastic strain field inside it.

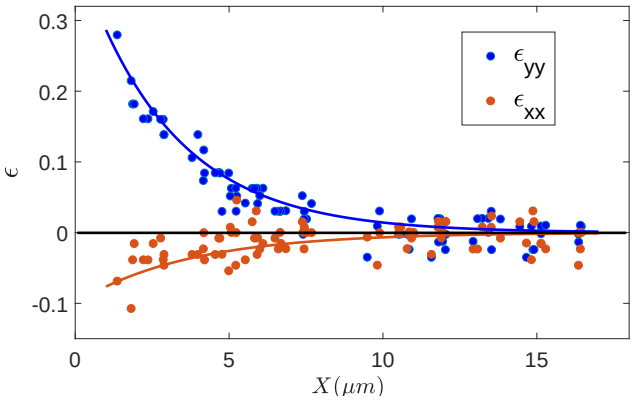

Fig. 7 Strain components ε_{yy} and ε_{xx} on the section oriented along the crack axis as a function of the distance X from the crack tip, as obtained from both the individual triad tracking analysis (dots) and the full DIC (lines).

‡ Let us note that the yield strain could be an underestimate of the elastic strain very close to the crack tip where strain hardening is likely to dominate the asymptotic stress field.

The smooth nature of the strain field in epoxys makes this material very promising for the application of the Digital Image Correlation (DIC) technique to measure the full strain field in the process zone as described in Ref.[21] DIC was successfully applied to the combined analysis of a selected series of 12 AFM images acquired at the same time each following day. The image series corresponds to a well conditioned steady-state crack propagation, with only minor long term variation of the propagation velocity. The differential strain measured by DIC analysis can thus be interpreted either as a strain rate (if divided over the time lag of $\Delta t \sim 1$ day) or as the spatial gradient of ε_{yy} along the direction of crack propagation x (if divided over the traveled distance $\Delta c \sim V\Delta t \sim 1$ µm). DIC analyses can be performed either incrementally between two consecutive images (1 day apart) as shown in Fig. 8(top), or spanning a longer interval of time (11 days here) as in Fig. 8(middle). It should be noted that the initial state is already much deformed by the presence of the loaded crack as compared to the rest state. Nevertheless, assuming a steady-state strain field being advected by the crack tip, it is possible to estimate the total strain field from the rest state, even in the absence of an AFM image of the latter. Such a total strain field is shown in Fig. 8(bottom) and the complete description of the present DIC procedure is detailed in a separate publication Ref[22]. When extracting the section aligned with the crack axis, the ε_{yy} and ε_{xx} can be well adjusted by exponentials with a characteristic length of ~ 3 µm that turn out to be in very good agreement with the handmade strain profiles as shown in Fig. 7.

This analysis reveals that under steady-state propagation condition the crack tip strain field presents two highly active regions forming an angle of about 38° to the crack propagation axis. The overall features of the measured process zone strain rate field are evocative of the Von Mises stress fields associated to plane stress LEFM solutions expected at the sample surface[23]. The forward tilt of the lobes is related to the negative T-stress values associated to the compressive condition of the DCDC geometry[7,24]. It is to be stressed that the most important difference with respect to crack tip fields obtained for the monotonic loading of a non-propagating crack, is that in steady-state propagation the maximum attained plastic strain remains stuck in a wake region left behind by the propagating process zone (see Fig. 8(bottom)).

The differential DIC analysis was performed between 12 consecutive steps. The measured strain rate field was observed to be very stable despite the 8% reduction in the force (and thus in K_C) and the reduction in the crack propagation velocity by a factor 6. This confirms that the maximum strain ε_{max} at the crack tip is very weakly dependent on the crack propagation velocity in the observed range of the $K_C(V)$ curve.

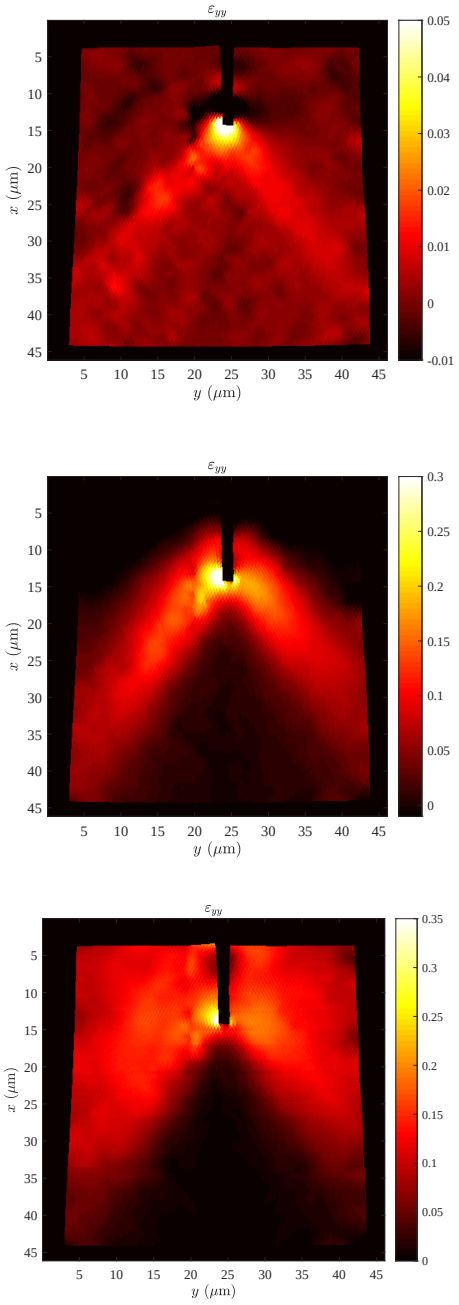

Fig. 8 DIC analysis of the strain field ε_{yy} between the 50 μm size AFM images obtained by using the software Correli^{LMT} [21]. (top) Incremental field between two consecutive images separated by crack propagation of about 1 μm. (middle) Cumulative strain in the whole image series of 12 images. (bottom) Reconstruction of the total plastic strain field from the rest state.

3 Unified model for the fracture toughness of glassy polymers

In this section we propose a unified scenario for steady-state and stick-slip fracture propagation in glassy polymers and build an approximate model by starting with the crack velocity dominated behavior and connecting it with the sample loading rate dominated response through a local process zone that governs failure.

The present in-situ AFM investigation with nanometric resolution has shown for the first time that for brittle thermosets like epoxy resin, a steady-state slow crack propagation behavior can be observed and characterized by a $K_C(V)$ curve, in a comparable way as for thermoplastics, although with a very low velocity limit V_{max}. An important complementary observation by Takahashi and Arakawa [10] has allowed to characterize the dynamic crack propagation in epoxy resins as a $K_C(V)$ curve with V systematically larger than 100 m/s, which is difficult to be measured during stick-slip dynamics, even with a fast camera. Moreover, Bonamy and coworkers [25,26] have developed an advanced loading fixture that allowed to show that PMMA can also present stick-slip dynamics under rapid loading conditions. The combination of all these observations suggests that the steady-state crack propagation curve $K_C(V)$ and the characteristic stick-slip curve $K_{start}(\dot{\delta})$ are two complementary facets of a unified crack propagation physics for all glassy polymers, in an analog way to what is observed in the peeling of adhesive tapes [27].

However, the link between these two curves is not trivial. In the classical picture, stick-slip dynamics is represented as the red cycle on the $K_C(V)$ curve in Fig. 9, where the change of slope in the $K_C(V)$ curve induces a crack propagation instability [27] (cf. § 3.3). According to this model, K_{start} is identified with the peak value K_{max} at the end of the slow quasi-static branch of the $K_C(V)$ curve and K_{stop} with the minimum value K_{min} of the dynamic branch. However, this picture can not account for the observed reduction of K_{start} with the sample loading velocity $\dot{\delta}$ as represented in Fig. 1(bottom) for epoxy resins.

A unified scenario is now proposed to link the $K_C(V)$ and $K_{start}(\dot{\delta})$ curves based on the insights of the in-situ AFM microscopic investigation of the strain fields associated with crack propagation, as well as on recent developments on the fracture of soft dissipative materials [12]. The relevant space, time and strain scales of the process-zone are extracted from the AFM images. The energy dissipation associated with crack propagation is estimated based on the finite strain viscoplastic behavior of the glassy polymer, which is characterized via uniaxial compression tests as a function of the strain rate $\dot{\varepsilon}$ (cf. Fig. 2 and Ref. [13]). The model will be formulated in terms of a more fundamental curve for the fracture energy $\Gamma(\dot{\varepsilon}_{PZ})$, where $\dot{\varepsilon}_{PZ}$ is a characteristic strain rate at the scale

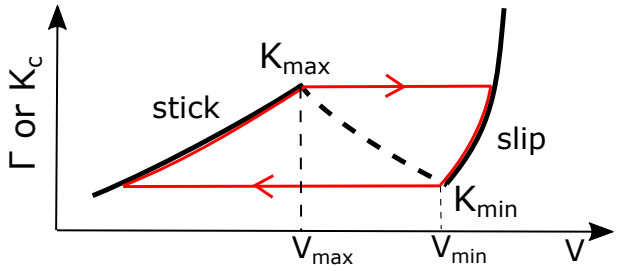

Fig. 9 Classical representation of stick-slip dynamics as a cycle (in red) on the $K_C(V)$ curve of steady-state fracture propagation. When the applied loading rate $\dot{\delta}$ corresponds to a steady-state velocity laying in the intermediate unstable negative slope branch (cf. Appendix), the crack propagation becomes a jerky alternation of slow and fast phases. In the slow phase (named 'stick') the crack propagation is so weak that K increases due to the external loading rate up to K_{max}, where the crack velocity jumps to the dynamic branch. In the fast phase (named 'slip') fast crack propagation over a finite crack length increment leads to sharp drop of K down to K_{min}, where the crack velocity drops.

of the process zone, that can be expressed in terms of both the crack propagation velocity V and the sample loading rate $\dot{\delta}$. The following sections focus on limiting cases where $\dot{\varepsilon}_{PZ}$ is dominated either by V (§3.1) or $\dot{\delta}$ (§3.2) and then the more general condition where a competition exists between the two (§3.3).

3.1 Model for $K_C(V)$ in steady-state crack propagation

The classical fracture propagation curve $K_C(V)$ is defined under steady-state crack propagation conditions, which means a constant stress intensity factor $\dot{K} = 0$. Since the process zone has a finite size R_{PZ} (cf. Fig. 10)[§], the steady-state crack propagation velocity V can only be established after the crack has traveled a distance that spans several times R_{PZ} under constant loading conditions. Thus a characteristic time t_{PZ} is proposed:

$$t_{PZ} \sim \frac{R_{PZ}}{V} \tag{2}$$

below which steady-state fracture cannot be defined. Once the crack propagation has been observed over a long enough time $t^* \gg t_{PZ}$, the steady-state crack tip strain field is well established and it propagates at a constant velocity V. This allows mapping spatial gradients of the strain fields along the crack propagation direction x into temporal strain rates at a given material point:

$$\varepsilon(x,t) = \varepsilon(x - Vt) \qquad \frac{\partial \varepsilon}{\partial t} \sim V \frac{\partial \varepsilon}{\partial x} \tag{3}$$

§ It should be stressed here that the circular shape in the sketch of the process zone is a rough simplification for representing the characteristic size of the process zone with no reference to a specific material behavior.

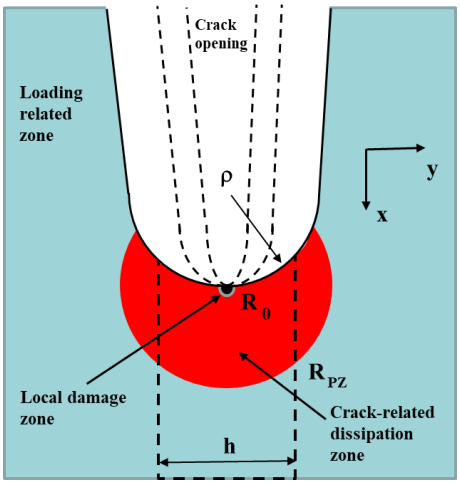

Fig. 10 Sketch of the lengthscales associated to crack propagation and energy dissipation in soft dissipative materials[12]. The small black region R_0 represents the intrinsic damage region, where the final rupture of the polymer network occurs. The red region R_{PZ} represents the process zone where viscoplastic energy dissipation is dominated by the propagating crack tip. The crack tip blunting radius ρ represents the region affected by large strain (plastic strain for glassy polymers). The width h of the sample (very large here) is represented for comparison with both R_{PZ} and ρ.

Based on the present in-situ investigation (cf. Figs. 7-8) and the characteristic picture of the process zone scales in Fig. 10, the strain field is described at the scale of the process zone (red region) as a constant spatial gradient of plastic strain ε^p up to a finite maximum strain ε^p_{max} at the crack tip (black region). This allows to estimate a characteristic strain rate $\dot{\varepsilon}^{steady}_{PZ}$ in the process zone under steady-state crack propagation using (2) and (3):

$$\dot{\varepsilon}^{steady}_{PZ} \sim \frac{\varepsilon^p_{max}}{t_{PZ}} \sim \frac{\varepsilon^p_{max} V}{R_{PZ}} \tag{4}$$

where all the quantities can be measured by the in-situ AFM observations.

The typical value for the volume density of dissipated work in the process zone is thus:

$$\mathcal{W}^{steady}_{diss}(\dot{\varepsilon}^{steady}_{PZ}) \sim \int_0^{\varepsilon^p_{max}} \sigma_{eq}(\varepsilon^p, \dot{\varepsilon}^{steady}_{PZ}) d\varepsilon^p \tag{5}$$

where the elasto-plastic constitutive behavior of the polymer can be measured by compressive tests and characterized by the hardening function $\sigma_{eq}(\varepsilon^p, \dot{\varepsilon})$, which relates the equivalent Von Mises stress σ_{eq} to the plastic strain ε_p for a given strain rate $\dot{\varepsilon}$.[28] For the sake of simplicity, the effect of hydrostatic stress on the hardening function is neglected, since it has only a second order effect for glassy polymers[20].

According to Fig. 10, the quasi-static fracture energy $\Gamma(V)$ can be split into an intrinsic fracture energy Γ_0 needed to break the molecular network at nanometer scale (black region) and a dissipative term $\Gamma_{diss}(V)$ that represents the visco-plastic dissipation at the micrometric scale of the process zone R_{PZ} (red region)[¶]:

$$\Gamma(V) = \Gamma_0 + \Gamma_{diss}(V) \tag{6}$$

The dissipative term $\Gamma_{diss}(V)$ can be estimated by considering the energy balance per unit surface over a basic steady-state propagation unit $dc \sim R_{PZ}$. This involves multiplying the typical volume density (5) by the volume of the process zone bR_{PZ}^2 and dividing it by the cross sectional area bR_{PZ}, where $b = 2t$ is the transverse dimension of the sample:

$$\begin{array}{c} \Gamma_{diss}(V) \sim R_{PZ} \mathcal{W}_{diss}^{steady}(\dot{\varepsilon}_{PZ}^{steady}) \sim \\ \sim R_{PZ} \int_0^{\varepsilon^p_{max}} \sigma_{eq}(\varepsilon^p, \dot{\varepsilon}_{PZ}^{steady}) d\varepsilon^p \end{array} \tag{7}$$

where $\dot{\varepsilon}_{PZ}^{steady}$ is related to the crack velocity V by (4). It should be stressed that this argument is limited to the situations where the sample width h is much larger than the process zone size R_{PZ}. Moreover, if a more realistic non circular description of the process zone is considered, the R_{PZ} in Eq. (7) should be replaced with the width of the process zone in the direction orthogonal to the fracture plane (direction y).

As argued in the next section, the intrinsic term Γ_0 can be measured through the crack arrest value of K_{stop}. The quasi-static fracture energy curve is thus obtained through (6) and it can then be converted into the toughness curve $K_C(V)$, which is more frequently used in the glassy polymer community, by the equivalence relation:

$$K_C(V) \sim \sqrt{E\Gamma(V)} \tag{8}$$

For the sake of clarity in the presentation of the model for the fracture energy, all along section 3 the elastic modulus E is considered to be a material constant at the macroscopic scale of the sample, since this does not change the core of the model that is focused on the mechanical response inside the process zone.

The present parameterless approach provides a descriptive modeling for the steady-state fracture toughness $K_C(V)$ of glassy polymers. This is the first step towards a fully predictive model, that will require new physical ingredients for predicting the dependency of the maximum plastic strain attainable in the process zone $\varepsilon^p_{max}(\dot{\varepsilon})$ as a function of the local strain rate, and possibly of the local stress triaxiality. This is related to the material physical failure criterion at the very end of the crack tip at smaller scales than the process zone (the local damage region identified in black in Fig. 10). With this further ingredient, the model would be able to predict the critical velocity V_{max} for the inversion of slope of the $K_C(V)$ curve, which is associated with the onset of the stick-slip instability according to standard models (cf. Fig. 9). The critical velocity V_{max} has very different values for different glassy polymers and it is thus a very good physical quantity to test any predictive model for the $K_C(V)$ curve.

3.2 Model for $K_{start}(\dot{\delta})$ in stick-slip crack propagation

Let us now consider the ideal case of unstable dynamic initiation of a pristine[‖] static crack of length c during monotonic sample loading at a rate $\dot{\delta}$. Let us suppose for simplicity that no crack propagation occurs during the loading of the sample up to the initiation toughness K_{start}, i.e. $\dot{c} = 0$ as in a classical 'stick' phase. The loading rate $\dot{K}$ of the process zone is thus simply proportional to the loading rate $\dot{\delta}$ of the sample (cf. Appendix).

Under the hypothesis that for each value of K the strain field developed in the process zone has essentially the same shape as the one observed for steady-state crack propagation, the strain rate of the process zone $\dot{\varepsilon}_{PZ}^{stick}$ can safely be assumed to be a monotonically increasing function of $\dot{K}$ and thus of the sample loading rate $\dot{\delta}$. The material physical failure criterion at the very end of the crack tip (black region) can also be assumed to remain the same, characterized by $\varepsilon^p_{max}(\dot{\varepsilon})$ as defined in previous section. The volume density of dissipated work and the different terms of the fracture energy can therefore be evaluated with the same eqs. (5,6,7):

$$\Gamma_{start}(\dot{\delta}) \sim \Gamma_0 + R_{PZ} \int_0^{\varepsilon^p_{max}} \sigma_{eq}(\varepsilon^p, \dot{\varepsilon}_{PZ}^{stick}) d\varepsilon^p \tag{9}$$

where this time $\dot{\varepsilon}_{PZ}^{stick}$ is related to the loading rate $\dot{\delta}$ (instead of V, which is vanishing here) by:

$$\dot{\varepsilon}_{PZ}^{stick} \sim \dot{\varepsilon}_{tip} = \frac{d\varepsilon_{tip}}{dK}\dot{K} = \frac{d\varepsilon_{tip}}{dK} B_K(c)\dot{\delta} \tag{10}$$

where the relationship $\varepsilon_{tip}(K)$ should either be modeled by finite elements or measured through an AFM investigation during the stick phase. $\Gamma_{start}(\dot{\delta})$ can then be converted to $K_{start}(\dot{\delta})$ by eq. (8). As for now, in order to provide approximated estimates of $\dot{\varepsilon}_{PZ}^{stick}$ with the available data, the experimental measurements of K_{start} and K_{stop} in stick-slip dynamics[9] can be used as follows:

$$\dot{\varepsilon}_{PZ}^{stick} \sim \frac{\varepsilon^p_{max}}{t_{stick}} \sim \frac{\varepsilon^p_{max}}{K_{start} - K_{stop}} B_K(c)\dot{\delta} \tag{11}$$

¶ The kinetic energy term in the energy balance is here neglected since the center of the dissipation peak for glassy polymers occurs at a crack propagation V_{max} well below the wave speed of $\sim$ 100 m/s. When necessary, standard dynamic fracture arguments[29] will be followed for dealing with the fast fracture branch.

‖ By 'pristine' it is meant that the crack neighborhood has not been previously affected by plastification. This is supposed to be the case for a crack arrested after dynamic propagation.

This can be justified by the following arguments. During a typical stick-slip regime, the loading phase ('stick') always happens after a previous cycle where the crack has arrested at a finite loading K_{stop}, which is experimentally independent from $\dot{\delta}$ and T.[11] The crack arrest occurs at K_{min} (cf. Fig. 9) after dynamic crack propagation[**], where plastic dissipation tends to vanish. Therefore, both terms $\Gamma_{stop} = \Gamma_{min}$ can be identified with the intrinsic fracture energy Γ_0 needed to break the molecular network at nanometer scale (black region in Fig. 10). After each crack arrest, the crack tip is very sharp due to the very small plastic deformation. Then a new loading cycle starts again in conditions very similar to a pristine crack.

In summary, it is proposed that both the steady-state curve $K_C(V)$ and the stick-slip curve $K_{start}(\dot{\delta})$ arise from the same fracture energy relation $\Gamma(\dot{\varepsilon}_{PZ})$. But the stick-slip branch corresponds to a higher range of strain rates $\dot{\varepsilon}_{PZ}$ (cf. next section) where the slope of the dissipation term $\Gamma_{diss}(\dot{\varepsilon}_{PZ})$ becomes negative, as it is typically the case due to the rheology of viscoelastic and viscoplastic materials. While the constitutive stress-strain laws generally have a monotonically increasing dependency of stress with strain rate[30], the maximum strain at failure $\varepsilon^p_{max}(\dot{\varepsilon})$ has a more complex behavior that depends on the specific physics of failure of each material[31,32]. When stick-slip is observed after some critical loading rate $\dot{\delta}_{max}$ (corresponding to V_{max} in Fig. 9, cf. Appendix), this means that $\Gamma(\dot{\varepsilon}_{PZ})$ changes from positive to negative slope after some critical strain rate $\dot{\varepsilon}^{max}_{PZ}$. This can only happen if the failure strain ε^p_{max} decreases faster with strain rate than the concomitant increase of stress, according to eq. (7). In other words, the negative slope $K_{start}(\dot{\delta})$ stick-slip curve provides experimental access to the negative slope branch of the $K_C(V)$ steady-state curve, which is not directly measurable due to its intrinsic instability.

In this second modeling section, it is assumed that there is no crack propagation during the loading phase of the stick-slip regime, so that the crack propagation does not follow the $K_C(V)$ curve up to its constant maximum K_{max} as sketched in the standard picture in Fig. 9. This allows to explain why $K_{start}(\dot{\delta})$ is a decreasing function of $\dot{\delta}$, which is a major point that lacked a sound interpretation in the literature.

The more general condition where both crack propagation and sample loading rate are simultaneously present will be discussed in next section.

[**] Let us note that in the 'slip' phase, the crack always follows the dynamic branch of the steady-state $K_C(V)$ curve, since the micrometric process zone size R_{PZ} is renewed thousands of times in any macroscopic crack propagation ($\Delta c \gg R_{PZ}$).

3.3 Competition between crack propagation and loading rate

Our present observations demonstrated the occurrence of slow crack propagation during what is called the 'stick' phase. Thus if a ramp loading of the sample at a rate $\dot{\delta}$ is considered, the most general condition is that both slow crack propagation and macroscopic loading contribute to the local strain rates in the process zone $\dot{\varepsilon}_{PZ}$, which in turn determines the fracture energy dissipation term $\Gamma_{diss}(\dot{\varepsilon}_{PZ})$. However, for slow loading rates the local strain rate $\dot{\varepsilon}_{PZ}$ will be dominated by the crack propagation velocity V, while for fast loading rates $\dot{\varepsilon}_{PZ}$ will by dominated by the loading rate itself.

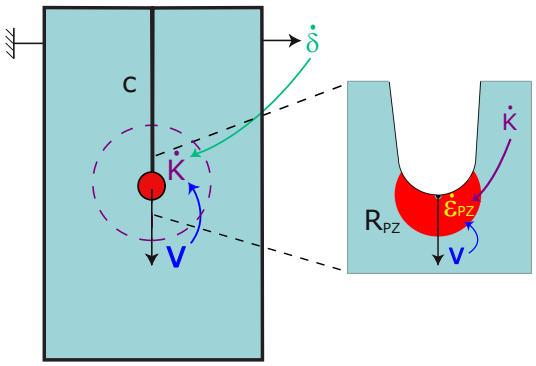

Fig. 11 Sketch of the two-scale competition between crack propagation and loading rate. At the macroscopic scale of the sample (left) the competition between the macroscopic loading rate $\dot{\delta}$ (green) and the crack propagation velocity V (blue) determines the crack tip loading rate $\dot{K}$ (violet) that enters the process zone. At the mesoscopic process zone scale (right) a second competition between the mesoscopic loading rate $\dot{K}$ and the crack propagation velocity V determine the caractristic strain rate ε_{PZ} (yellow) of the process zone.

Indeed the competition between crack propagation and loading rate happens at two different scales as sketched in Fig. 11. At the macroscopic scale of the sample the loading rate tends to increase K, while crack propagation tends to reduce it, so that steady-state propagation in a sample like Double Torsion[33] (which is frequently used for stick-slip tests in epoxys, cf. Appendix for mathematical treatment of this and more general samples) requires that:

$$\frac{\dot{K}}{K} = \frac{\dot{\delta}}{\delta} - \frac{\dot{c}}{c} = 0 \tag{12}$$

The macroscopic steady-state condition on K defines a structural equivalence between $\dot{\delta}$ and the crack propagation velocity $V = \dot{c}$:

$$\dot{\delta} = \frac{\delta}{c} V \tag{13}$$

The stick-slip instability appears when the sample loading rate exceeds a first critical value $\dot{\delta}_{max} = \frac{\delta}{c} V_{max}$, which corresponds to the local maximum of the $\Gamma(V)$ curve in Fig. 9

where the slope changes from positive to negative. The stick-slip disappears when the sample loading rate exceeds a second critical value $\dot{\delta}_{min} = \frac{\delta}{c} V_{min}$ corresponding to the local minimum of $\Gamma(V)$ where the slope goes back positive.

In the stick-slip regime, the equivalence condition (13) is permanently violated. On the one hand, during the 'stick' phase, the crack velocity V is smaller than the equivalent loading rate $(c/\delta)\dot{\delta}$, and K will increase according to (12). In particular, when $\dot{\delta} \gg \dot{\delta}_{max}$ the positive $\dot{K}$ is essentially dominated by the sample loading rate $\dot{\delta}$:

$$\frac{\dot{K}}{K} = \frac{\dot{\delta}}{\delta} > 0 \tag{14}$$

On the other hand, during the 'slip' phase, the crack velocity V is larger than the equivalent loading rate $(c/\delta)\dot{\delta}$, and K will decrease according to (12). In particular, when $\dot{\delta} \ll \dot{\delta}_{min}$ the negative $\dot{K}$ is rather dominated by the fast crack propagation velocity $V = \dot{c}$:

$$\frac{\dot{K}}{K} = -\frac{V}{c} \tag{15}$$

The first part of this section dealt with the classical competition between crack propagation V and loading rate $\dot{\delta}$ at the macroscopic scale of the sample in order to determine the local loading rate $\dot{K}$ that is perceived by the process zone (cf. Fig. 11(left)). In the second part of the section, a second competition happening at the microscopic scale can be examined, where the crack propagation V and the local loading rate $\dot{K}$ compete in order to determine the average strain rate $\dot{\varepsilon}_{PZ}$ inside the process zone (cf. Fig. 11(right)).

When eq. (12) is not obeyed, a characteristic time of variation of K can be defined:

$$t_K = \left|\frac{K}{\dot{K}}\right| = \left|\frac{\dot{\delta}}{\delta} - \frac{V}{c}\right|^{-1} \tag{16}$$

which is valid for both increasing and decreasing K.

As discussed in section 3.1, the $K_C(V)$ curve describes crack propagation when the average strain rate $\dot{\varepsilon}_{PZ}$ at the process-zone scale is dominated by the crack propagation velocity V. This implies that the effects of the loading rate $\dot{K}$ should be negligible over an observation time $t^* \gg t_{PZ}$, cf. eq. (2), which can be stated as the condition:

$$t_K \gg t^* \gg t_{PZ} \tag{17}$$

which is called the 'V-dominance' condition hereafter.

When the opposite inequality is fulfilled, then the loading K will change significantly before the crack tip has advanced by any significant fraction of the process-zone. Crack propagation can thus be neglected and the average strain rate $\dot{\varepsilon}_{PZ}$ at the process-zone scale is dominated by the loading rate $\dot{K}$, which is called '$\dot{K}$-dominance' condition in the following. Although some crack propagation is still present, fracture propagation is not any more described by the $K_C(V)$ curve, but it can still be considered to be ruled by the relationship $\Gamma(\dot{\varepsilon}_{PZ})$. In particular, when the '$\dot{K}$-dominance' condition occurs during the loading phase of stick-slip dynamics, this can lead to the crack initiation curve $K_{start}(\dot{\delta}) < K_{max}$ that was discussed in section 3.2.

Let us now consider the link between this understanding and the classical picture of stick-slip dynamics sketched in Fig. 9. In order for crack propagation to follow the red cycle on the $K_C(V)$ curve, the V-dominance condition should be fulfilled during the whole cycle. While this is likely to be the case for the slip phase, where V is dynamic and t_{PZ} is very short[††], the V-dominance condition is likely to be violated during the stick phase where crack propagation is very slow. However, as the loading is progressively increasing, the V-dominance condition could still be attained before reaching the instability at V_{max}. The remaining part of the stick phase would then be ruled by the $K_C(V)$ curve up to K_{max}. The instability leading to the slip phase would thus occur at a constant value $K_{start} = K_{max}$ independent of the loading rate $\dot{\delta}$ as in the classical picture. In order for this not to happen, the V-dominance condition should remain violated up to the critical velocity V_{max}. The strain rate of the process-zone $\dot{\varepsilon}_{PZ}$ would thus remain dominated by the loading rate $\dot{\delta}$ up to the unstable crack initiation, leading to the variable $K_{start}(\dot{\delta})$ curve that is frequently observed.

A conservative estimate for the transition from the classical K_{max} behavior to the $K_{start}(\dot{\delta})$ curve is written as follows:

$$\begin{aligned} \left|\tfrac{K}{\dot{K}}\right| = t_K(V_{max}) < t_{PZ}(V_{max}) = \tfrac{R_{PZ}}{V_{max}} \\ \tfrac{\dot{\delta}}{\delta} - \tfrac{V_{max}}{c} > \tfrac{V_{max}}{R_{PZ}} \\ \tfrac{\dot{\delta}}{\delta} > V_{max}\left(\tfrac{1}{c} + \tfrac{1}{R_{PZ}}\right) \simeq \tfrac{V_{max}}{R_{PZ}} \end{aligned} \tag{18}$$

4 Discussion

4.1 The unified model

According to the unified modeling presented in section 3, the steady-state curve $\Gamma(V)$ and the stick-slip curve $K_{start}(\dot{\delta})$ observed for epoxy resins are two different expressions of the

†† Concerning the 'slip' phase, where dynamic branch has both a very fast velocity V and a very fast unloading rate $\dot{K} < 0$ it is convenient to think of the steady-state condition (2) in terms of traveled distance: $dc_{PZ} \gg R_{PZ}$. Since the rapid drop of K happens over a finite slip amplitude Δc, then the V-dominance condition will generally be fulfilled if the amplitude of the slip is larger than a process zone size: $\Delta c \gg R_{PZ}$. While this is comfortably satisfied when $K_{start}(\dot{\delta}) > K_{stop}$, it can be questioned when the stick-slip amplitude is vanishing in the pseudo-'stable' regime at high $\dot{\delta}$.

same process zone mechanism. Both can be related to the measured constitutive viscoplastic behavior $\sigma_{eq}(\varepsilon^p, \dot{\varepsilon})$, but in the first case the relevant strain rate of the process zone is determined by the crack propagation velocity V, while for the second it is determined by the loading rate $\dot{\delta}$. Let us emphasize that this modeling is presently rather speculative, yet it does not possess any adjustable parameter and it is thus formulated in such a way that it can be experimentally tested by combining in-situ AFM techniques and rheological measurements on several different glassy polymers. Although this modeling is quite rough at present, its consistency with the available data for fracture propagation and rheology in glassy polymers can already be assessed as well as its compatibility with the existing knowledge about the mechanisms of fracture propagation in these materials.

4.2 $\Gamma(V)$ curve

When considering typical values of the quantities measured for glassy polymers we can obtain $\Gamma_{diss} \sim R_{PZ}\sigma_y\varepsilon^p_{max} \sim 10$ μm $\times$ 100 MPa $\times$ 0.3 $\sim$ 300 J/m^2, and $K_C \sim \sqrt{E\Gamma} \sim \sqrt{3 \text{ GPa} \times 300 \text{ J/m}^2} \sim 1$ MPa m$^{1/2}$, which provide the good orders of magnitude for the fracture energy and toughness. In principle, R_{PZ} and ε^p_{max} depend on the crack velocity V through the strain rate $\dot{\varepsilon}_{PZ}$. However, glassy polymers are only weakly viscoplastic at ambient temperature due to their elevated glass transition temperature above 100°C. The process zone size and crack opening displacement $\delta_{COD} \sim R_{PZ} \cdot \varepsilon^p_{max}$ in PMMA were observed to be only weakly variable functions over many decades of crack velocity (cf. Ref[5] and Fig. 1(top)). In agreement with this observation, the present in-situ AFM investigation has not revealed any significant change in the steady-state strain field of the process zone after the crack propagation velocity decreased by one decade. Thus the small slope of the $\Gamma(V)$ curves should be related to the weak dependency of the constitutive behavior $\sigma_{eq}(\varepsilon^p, \dot{\varepsilon})$ with respect to the strain rate $\dot{\varepsilon}$. According to eq. (4) the range of strain rates $\varepsilon^{steady}_{PZ}$ in the process zone explored by the in-situ AFM investigation is between 10^{-7} and 10^{-5} s^{-1}, the latter corresponding to the estimate of the upper limit of the steady-state crack propagation. As it can be observed in Fig. 6, K_c increases by about 20% over these two decades of velocity, which corresponds to a very weak power law exponent of 0.04. The same power law exponent describes the increase of the yield stress with the strain rate as reported in Table 1, although the available range of strain rate in the macroscopic tests (10^{-3} to 10^{1} s^{-1}) is well above the strain rates explored in the very slow crack propagation. Within the present level of overall experimental precision, no more than an order of magnitude of Γ can be estimated as well as the approximate slope of $\Gamma(V)$ for each measured polymer. A thorough experimental validation of this approach will require measurements on several different polymers with significantly different rheological properties, that should be characterized over a wider range of strain rates and temperatures.

It is very encouraging that the present approach has provided a very good description of the adherence energy curves $\Gamma(V,T)$ for the peeling of adhesive tapes with custom nonlinear rheology as presented in Ref[31]. The main difference between the two models is that since the adhesive thickness h is much smaller than the process zone size R_{PZ} (cf. Fig. 10), the integration of the energy density in eq. (7) should be limited to h instead of R_{ZP}. This leads to the peculiar property that adherence energy is proportional to the adhesive thickness.

4.3 Interpretation of K_{stop} and Γ_0

Let us now focus on the physical interpretation of the Γ_0 term corresponding to the intrinsic fracture energy needed to break the molecular network at nanometer scale and its link to the available measurements of K_{stop}. Following the arguments of section 3.2, the crack arrest condition K_{stop} occurs at the end of a slip phase where dynamic fracture occurs at velocities above 100 m/s for glassy polymers and plastic yield should be quite limited. It should thus be identified both with the minimum K_{min} of the dynamic branch (due to 'V-dominance') and to the intrinsic fracture energy Γ_0. These conclusions are consistent with the observed insensitivity of K_{stop} to both the loading rate $\dot{\delta}$ and temperature T.[11] Moreover, they are consistent with the observed lower limit saturation of $K_{start}(\dot{\delta}, T)$ to the value of K_{stop} when increasing the loading rate $\dot{\delta}$ (or decreasing temperature) that is shown in Fig. 1(bottom). According to our modeling and our in-situ observations, $(\Gamma_{start} - \Gamma_{stop})$ should thus be identified with the viscoplastic dissipation Γ_{diss}, associated to the plastic blunting of the process zone prior to the nucleation of a new dynamic crack, in agreement with the conclusions of other authors[9,34].

We remark that both experimental values of Γ_{stop} and Γ_{min} are of the order of 100 J/m^2,[9,26] which has the same order of magnitude as the plastic dissipation term Γ_{diss} in the stick-slip regime. This large value may appear as surprising for modeling the intrinsic fracture energy at nanometer scale, where typical covalent bond energies correspond to about 1 J/m^2.[11] However, let us stress that glassy polymers are made of polymer networks where random chains are coiled between chemical crosslinks or entanglements. Although the polymers are glassy and chain mobility is weak at ambient temperature, it is sound that the rupture of covalent bonds also involves local tension of polymer chains before rupture in a similar way to what happens in rubbers. This energy dissipation mechanism, called Lake-Thomas model for rubbers[35], implies the loss of the whole stretch energy of the chain, which can justify typical values of 100 J/m^2 such as observed for Γ_0 in non-viscoelastic

rubbers[35]. Moreover, although K_{stop} is quite insensitive to most material parameters for epoxy resins, it was observed to be correlated to the square root of the mass M_c between crosslinks[36], which is a typical signature of the Lake-Thomas mechanism.

4.4 Shear lips

Although the present approximate modeling does not explicitly account for the shear concentration regions observed during both steady-state (our investigation) and stick-slip[34] fracture propagation, their contribution to the energy dissipation can easily be integrated in the model. The measured strain field on Fig. 8 shows that across the shear lips (whose width is approximately 10 μm) a total shear strain of about 0.1 is observed. The lip width is similar to the size of the roughly circular confined process zone that was considered in the model and explored by the section in Fig. 7. Since the whole field propagates at a constant velocity, the typical strain field in the shear lips is very close to the previous estimates, i.e. 10^{-7} s^{-1} for $V = 10$ pm/s. The viscoplastic behavior (and σ_y) should thus be similar. In order to evaluate the contribution of the shear lips to the fracture energy, a similar equation to (7) can be used, but using the width h_L spanned by the shear lips in a direction normal to the crack propagation direction instead of R_{PZ}. Although $h_L \sim 100$ μm is larger than $R_{PZ} \sim 10$ μm, the maximum plastic deformation involved in the shear lips is smaller, and it decreases with the distance from the crack tip. Thus the shear lips contribute to the energy dissipation term with a similar order of magnitude as the confined process zone. Moreover, the dependency on both crack propagation velocity and loading rate $\dot{\delta}$ should be similar. In future developments, the in-situ AFM analysis of the strain fields associated to the shear lips will provide important fine evaluations of the dissipated energy, especially when combined with finite element modeling.

It should be noted that although thermosets frequently present unstable shear localization into shear bands with well defined contours of shear discontinuity, the incremental strain fields measured by the present DIC analysis reveal a smooth strain concentration field that propagates in steady-state along with the crack tip. This observation is consistent with the absence of appreciable post-yield strain softening in the compressive behavior.

4.5 Features of stick-slip

Let us now consider the initial issue of why some polymers like PMMA generally present steady-state fracture, while most brittle epoxy resins essentially present stick-slip fracture with $K_{start}(\dot{\delta})$ behavior. Although many mechanical properties such as E, σ_y, R_{PZ} and Γ are similar for the two kinds of glassy polymers, our present measurements allowed to identify a steady-state branch for the epoxy resin, but with a maximum velocity $V_{max} \sim 1$ nm/s, which is seven orders of magnitude lower than the value of $V_{max} \sim 1$ cm/s for PMMA. These correspond to typical strain rates in the process zone respectively of 10^{-5} s^{-1} for epoxy and 10^{2} s^{-1} for PMMA. When using similar fracture test samples for the two materials, the equivalent loading rate $\dot{\delta}_{max}$ for the transition between steady-state and stick-slip (which is dependent on the kind of sample used and its dimensions, cf. Appendix) will also be seven orders of magnitude lower for epoxy resins. Since typical loading times are a few seconds to minutes, obtaining steady-state in PMMA and stick-slip in epoxy appear as expected. During our in-situ AFM measurements, the loading stage is arrested, and thus slow steady-state fracture in epoxy can comfortably be observed for several days.

Moreover, the previously proposed modeling also allows one to explain why the stick-slip observed by Hattali[26] for PMMA at higher loading rates has the classical behavior with a constant value of $K_{start} = K_{max}$ (as in Fig. 9), while epoxy resins present a decreasing function of the loading rate $K_{start}(\dot{\delta})$. When considering the V-dominance condition (17), the time to cross the process zone for PMMA at V_{max} is $t_{PZ} \sim 3$ ms, while it is 8 hours for epoxy (*seven* orders of magnitude larger!). When compared to the typical loading time of a few seconds or minutes, the V-dominance condition at instability (18) is generally fulfilled for PMMA, while it can not be fulfilled during the loading phase in epoxys. Crack propagation during loading in epoxy samples can only represent a minor fraction of the process zone and the strain rate $\dot{\varepsilon}_{PZ}$ is clearly dominated by $\dot{\delta}$ leading to the decrease of $K_{start}(\dot{\delta})$.

4.6 Dissipation peak and negative slope branch

Although there has been many debates on the existence of a negative branch in the $\Gamma(V)$ curve that is not experimentally accessible[4,37], our modeling allows for a natural interpretation of this negative branch in terms of a change of slope of the more general curve $\Gamma_{diss}(\dot{\varepsilon}_{PZ})$, which is related to sound physical properties by eq. (7) and to an equivalent crack propagation velocity V by eq. (4). Moreover, this modeling endows the $K_{start}(\dot{\delta})$ curve with the status of a measurement of the negative branch of the $\Gamma(V)$ curve. A typical strain rate associated to the typical loading times of seconds to minutes during the stick phase of a well developed stick-slip regime in epoxy resin is about 10^{-3} s^{-1} to 10^{-1} s^{-1}.[11] This intermediate strain rate range is consistently comprised between the upper limit of the strain rates of 10^{-5} s^{-1} explored in the slow steady-state branch (cf. Fig. 6), and the lower limit of the strain rates of 10^{-1} s^{-1} where the stick-slip amplitude vanishes and a stable propagation velocity larger than 10^{-5} m/s

can be observed again[11]. Further development of the present modeling, including new physical insights on the failure criterion inside the process zone $\varepsilon^p_{max}(\dot{\varepsilon})$, can lead to predict the critical velocity V_{max} for the change of slope of the $\Gamma(V)$ curve. This would allow to explain why this important property can change as much as seven orders of magnitude for two glassy polymers that present overall similar mechanical properties.

Alternative interpretations exist in the literature for the peak in the $\Gamma(V)$ curve and the related instability. In particular, Williams[38] proposed an interpretation based on the isothermal-adiabatic transition at the crack tip for PMMA. Although their calculation provides a sound alternative estimate of V_{max} for PMMA, this interpretation can not be extended to epoxy resins, where V_{max} is seven orders of magnitude smaller, and isothermal conditions are clearly fulfilled during slow crack propagation close to the instability.

Another possible physical origin to be considered for the instability is the nucleation of brittle dynamic cracks from random defects existing in the material close to the slowly propagating blunted crack front, which would be consistent with the highly metastable character of the terminal region of the $\Gamma(V)$ curve close to the instability. Only a systematic experimental testing on several glassy polymers will allow for discriminating between these different models.

5 Conclusion

By an original AFM in-situ investigation of the morphology of the process-zone of a loaded crack tip in a brittle epoxy, steady-state crack propagation was shown for the first time to occur in brittle epoxys, with propagation velocities smaller than nm/s, which were not accessible in previous investigations by optical microscopy.

Although this crack propagation velocity is too slow to measure the $K_C(V)$ curve by a standard load relaxation technique[39], a portion of the $K_C(V)$ curve for our brittle epoxy could successfully be measured by combining the intrinsic relaxation of the epoxy and the elevated velocity resolution of AFM, as developed in a previous paper[16]. The results obtained with three different samples with different crack length, were observed to be fully consistent with each other, showing that the $K_C(V)$ curve can provide a good characterization of slow fracture propagation for brittle epoxys in a similar way to what happens for other glassy polymers such as PMMA. Moreover, the measured $K_C(V)$ curve is quantitatively similar to that for PMMA on both the values of K_C and the small value of the slope, which highlights that the most important difference is in the value of the upper limit velocity V_{max}, which is seven orders of magnitude smaller for our brittle epoxy than for PMMA.

Combining the AFM images of the propagating crack tip at the scale of the micrometric process zone and digital image correlation, the viscoplastic strain fields associated with steady-state propagation could be characterized. In a very different manner from PMMA and polycarbonate where strong localization mechanisms are active in the process zone[3,16,40], the strain field in epoxy presents a smooth strain concentration when approaching the crack tip, which is consistent with the absence of appreciable post yield softening, reaching finite plastic strains of about 30% associated to significant crack tip blunting at the process zone scale of 10 micrometers. These finite strains, compatible with the maximum possible stretching of the polymer network, are well beyond the values that are sustainable at the macroscopic scale in the extension of such brittle materials. Moreover, two shear concentration lips are evidenced forming an angle of about 38° ahead of the crack, extending over few hundred micrometers. These are similar to what can be optically appreciated during the loading of a static crack, as observed by Phillips et al.[34] during stick-slip crack propagation, but our analysis shows that the shear lips are plastically active regions that propagate along with the crack tip. The propagation of these shear lips leads to an effective discontinuity in plastic shear that is necessary to accommodate the propagation of a heavily blunted crack tip with an incompressible plastic flow, leaving a permanently deformed wake zone behind the crack tip, in a similar way to what is observed in the cutting of metals with a wedge blade[41].

The similarity between the strain fields observed during the slow steady-state propagation and the loading phase of stick-slip crack propagation, combining blunting, finite strains and shear lips has led us to develop a common interpretation for modeling the fracture energy for both the $K_C(V)$ curve and the $K_{start}(\dot{\delta})$, based on a modeling philosophy that was recently developed for soft dissipative materials[12,31,42–45]. The model provides an estimate of the viscoplastically dissipated energy $\Gamma_{diss}(\dot{\varepsilon}_{PZ})$ based on a characteristic volume energy density associated to the finite strain of the blunt process zone at a characteristic strain rate $\dot{\varepsilon}_{PZ}$ that is obtained by combining the size of the process zone and the crack propagation velocity. On the one hand, for slowly changing macroscopic loading the typical strain rate in the process zone is driven by the steady-state propagation of the plastic strain field at the crack propagation velocity V, leading to a crack propagation criterion in the form $K_C(V)$. On the other hand, for rapid macroscopic loading, slow crack propagation can be neglected and the typical strain rate in the process zone is driven by the macroscopic loading rate $\dot{\delta}$. This second condition is frequently fulfilled during the loading phase of stick-slip crack propagation, leading to a crack propagation criterion in the form $K_{start}(\dot{\delta})$. The transition between the two regimes is associated with the comparison between a characteristic time of the loading rate t_K and the characteristic time

for the crack to cross the process zone $t_{PZ} = R_{PZ}/V$. This should not be confused with the transition between steady-state and stick-slip crack propagation that is associated with the velocity V_{max} where the slope of the viscoplastic dissipation term $\Gamma_{diss}(\dot{\varepsilon}_{PZ})$ changes from positive to negative, and which is very different between glassy polymers. Yet, the dominance transition is frequently happening during the stick-slip regime, especially for materials where V_{max} is very low, such as epoxy resins. The negative slope of $K_{start}(\dot{\delta})$ can thus be used to explore the unstable negative branch of the $\Gamma_{diss}(\dot{\varepsilon}_{PZ})$, which is not accessible through steady-state measurements. This negative slope branch is associated with an embrittlement transition as a function of increasing strain rate or reduced temperature, which should be further investigated by future modeling of the maximum strain for failure in the process zone. Let us stress that this scenario is very different from the classical stick-slip cycles based on the $K_C(V)$ curve, where K_{start} would be a constant value (cf. K_{max} in Fig. 9), which can only be observed below some critical loading rate predicted here.

In order to complete the model for the fracture energy, it is argued that for both steady-state and stick-slip fracture the plastic dissipation term should be added to an intrinsic fracture energy term Γ_0 that is needed to break the molecular network at nanometer scale. Arguments were provided to identify this term Γ_0 with both the lower threshold limit K_{min} of the $K_C(V)$ curve and the crack arrest value K_{stop} during stick-slip, which corresponds to the lower limit of the fast dynamic crack propagation branch. Let us emphasize that for most glassy polymers Γ_0 is quite large ($\sim$ 100 J/m^2) and is comparable with the magnitude of the plastic dissipation term. Such a high energy dissipation at the nanometric network scale is soundly associated with the peculiar work of stretching of polymer network chains before rupture as it is commonly accepted for rubbers[35].

While the present modeling is quite approximate, it has the advantage of being mostly based on measurable quantities made accessible by our in-situ investigation technique and that should be extended to a wider class of glassy polymers. On the one hand, future experimental developments will hopefully allow one to measure strain fields during the loading phase of stick-slip, where AFM measurements are very delicate due to the mechanical drifts of the sample during the loading. On the other hand, future developments of the modeling including finite element simulations should lead to a better understanding of the physics of propagation of the nanometric damage zone associated to the intrinsic fracture energy Γ_0, which is embedded into the soft dissipative process zone. This would allow to model the dependency of the maximum crack tip strain on the average strain rate and local stress triaxiality in the process zone, and thus to change the present modeling from a descriptive one to a predictive one. In particular this would allow to model the critical velocity V_{max} corresponding to the change of slope of the $K_C(V)$ curve that is very important for engineering the transition from steady-state to stick-slip crack propagation. Since V_{max} can change over many orders of magnitude between different glassy polymers, it can be a very important benchmark to discriminate between different physical models for the toughness curves.

Conflicts of interest

There are no conflicts to declare.

Acknowledgments

This work has been supported by the French ANR through grant PROMORPH ANR-2011-RMNP-006. We thank J.F. Gerard, J.W. Hutchinson, X. Morelle, E. Barthel and C. Creton for fruitful discussions. We thank the interns C. Greboval, A. Pickel and D. Poitevin for their contribution in the initial developments of this work.

Appendix: Equivalent loading rate

Let us consider the loading of a generic LEFM sample with a constant velocity $\dot{\delta}$ applied at the loading points, as sketched in Fig. 11(left). The linear response of the sample can be characterized by its elastic compliance $J(c)$ that depends on the crack length c:

$$\delta = J(c)F$$

which allows to write the strain energy release rate as:

$$G = \frac{1}{2b}\frac{\delta^2}{J(c)^2}\frac{dJ}{dc}(c)$$

and then to obtain the stress intensity factor:

$$K(c,\delta) = \sqrt{EG} = B_K(c)\delta \tag{19}$$

where $B_K(c)$ depends on the structure of the specific sample though $J(c)$:

$$B_K(c) = \sqrt{\frac{E}{2b}\frac{dJ}{dc}(c)}\frac{1}{J(c)} \tag{20}$$

By derivation of (19) the local loading rate $\dot{K}$ can be expressed as a function of both the external loading rate $\dot{\delta}$ and the crack propagation velocity $V = \dot{c}$:

$$\dot{K} = \frac{dB_K}{dc}\delta \cdot V + B_K(c)\dot{\delta} \tag{21}$$

The steady-state condition for fracture propagation ($\dot{K} = 0$), thus requires the following condition at the macroscopic scale:

$$\dot{\delta} = -\frac{\delta}{B_K(c)}\frac{dB_K}{dc}V = B_\phi(c)\delta \cdot V = \phi(V, c, \delta) \quad (22)$$

where $B_\phi(c)$ is a sample specific function that can be derived from $B_K(c)$ as:

$$B_\phi(c) = -\frac{1}{B_K(c)}\frac{dB_K}{dc} \quad (23)$$

The function ϕ defines an equivalence relation between the loading rate $\dot{\delta}$ and the propagation velocity V that corresponds to steady-state crack propagation for a given sample geometry.

This allows for example to express the critical loading rate $\dot{\delta}_{max} = \phi(V_{max})$ that corresponds to the transition between steady-state and stick-slip on a specific sample geometry. When substituting (22) back into (21), K increases when the loading rate $\dot{\delta}$ is larger than the loading rate equivalent to the crack propagation velocity:

$$\dot{K} = B_K(c)(\dot{\delta} - B_\phi(c)\delta \cdot V) \quad (24)$$

For fracture tests such as the Double Torsion, where the compliance is a linear function of the crack length $J(c) = B_J c$, equation (21) can be simplified to (12) as used in the main text.

References

1 J. G. Williams, *Fracture mechanics of polymers*, Ellis Horwood Series in Engineerign Science, New York, 1984, p. 302.

2 A. J. Kinloch, *Fracture behaviour of polymers*, Chapman and Hall, 1983, p. 482.

3 E. J. Kramer, *Crazing in polymers*, Springer, 1983, pp. 1–56.

4 D. Maugis and M. Barquins, *In: Allen KW, editor. Adhesion 12. London: Elsevier Applied Science*, 1988, **310**, 205.

5 W. Döll, *Crazing in Polymers*, Springer, 1983, pp. 105–168.

6 D. Dugdale, *Journal of the Mechanics and Physics of Solids*, 1960, **8**, 100–104.

7 K. Broberg, *International journal of fracture*, 1999, **100**, 133–142.

8 E. Sharon, S. P. Gross and J. Fineberg, *Physical Review Letters*, 1996, **76**, 2117.

9 A. Kinloch and J. Williams, *Journal of Materials Science*, 1980, **15**, 987–996.

10 K. Takahashi and K. Arakawa, *Exp. Mech.*, 1987, **27**, 195–199.

11 R. Gledhill, A. Kinloch, S. Yamini and R. Young, *Polymer*, 1978, **19**, 574–582.

12 C. Creton and M. Ciccotti, *Reports on Progress in Physics*, 2016, **79**, 046601.

13 Y. Nziakou, *PhD Thesis, Université Pierre et Marie Curie, Paris, France*, 2015.

14 R. Gledhill and A. Kinloch, *Polymer*, 1976, **17**, 727–731.

15 C. Janssen, *Revue de Physique Appliquée*, 1977, **12**, 803–803.

16 M. George, Y. Nziakou, S. Goerke, A.-C. Genix, B. Bresson, S. Roux, H. Delacroix, J.-L. Halary and M. Ciccotti, *Journal of the Mechanics and Physics of Solids*, 2018, **112**, 109–125.

17 K. Idonije, M. Motuku, I. Shehata and H. Aglan, *Journal of reinforced plastics and composites*, 1993, **12**, 778–786.

18 G. Pallares, L. Ponson, A. Grimaldi, M. George, G. Prevot and M. Ciccotti, *International journal of fracture*, 2009, **156**, 11–20.

19 T. A. Plaisted, A. V. Amirkhizi and S. Nemat-Nasser, *International journal of fracture*, 2006, **141**, 447–457.

20 J. L. Halary, F. Lauprêtre and L. Monnerie, *Polymer materials: macroscopic properties and molecular interpretations*, John Wiley & Sons, 2011.

21 Z. Tomičević, F. Hild and S. Roux, *The Journal of Strain Analysis for Engineering Design*, 2013, **48**, 330–343.

22 S. Roux et al., *In preparation*, 2021.

23 D. Maugis, *Contact, adhesion and rupture of elastic solids*, Springer Science & Business Media, 2013, vol. 130.

24 T. Fett, G. Rizzi and D. Munz, *Engineering fracture mechanics*, 2005, **72**, 145–149.

25 M. Hattali, J. Barés, L. Ponson and D. Bonamy, Materials Science Forum, 2012, pp. 920–924.

26 T. Vincent-Dospital, R. Toussaint, S. Santucci, L. Vanel, D. Bonamy, L. Hattali, A. Cochard, E. G. Flekkøy and K. J. Måløy, *Soft Matter*, 2020, **16**, 9590–9602.

27 D. Maugis, *Review subcritical crack growth, surface energy, fracture toughness, stick-slip and embrittlement*, 1985.

28 L. Anand and S. Govindgee, *Continuum Mechanics of Solids*, Oxford University Press, Oxford, 2020, p. 736.

29 L. B. Freund, *Dynamic fracture mechanics*, Cambridge university press, 1990.

30 C. G'sell and J. Jonas, *Journal of materials science*, 1979, **14**, 583–591.

31 J. Chopin, R. Villey, D. Yarusso, E. Barthel, C. Creton and M. Ciccotti, *Macromolecules*, 2018, **51**, 8605–8610.

32 V. Pandey, A. Fleury, R. Villey, C. Creton and M. Ciccotti, *Soft Matter*, 2020, **16**, 3267–3275.

33 M. Ciccotti, *Realistic Finite-Element Model for the Double-Torsion Loading Configuration*, 2000.

34 D. Phillips, J. Scott and M. Jones, *Journal of Materials Science*, 1978, **13**, 311–322.

35 G. J. Lake and A. Thomas, *Proceedings of the Royal Society of London A*, 1967, **300**, 108.

36 J. LeMay and F. Kelley, *Epoxy resins and composites III*, 1986, 115–148.

37 M. Ciccotti, B. Giorgini and M. Barquins, *International journal of adhesion and adhesives*, 1998, **18**, 35–40.

38 J. Williams, *International Journal of Fracture Mechanics*, 1972, **8**, 393–401.

39 M. Ciccotti, N. Negri, L. Sassi, G. Gonzato and F. Mulargia, *Journal of volcanology and geothermal research*, 2000, **98**, 209–217.

40 A. M. Donald and E. J. Kramer, *Journal of Materials Science*, 1981, **16**, 2967–2976.

41 T. Atkins, *The science and engineering of cutting: the mechanics and processes of separating, scratching and puncturing biomaterials, metals and non-metals*, Butterworth-Heinemann, 2009.

42 R. Villey, C. Creton, P. Cortet, M. Dalbe, T. Jet, B. Saintyves, S. Santucci, L. Vanel, D. Yarusso and M. Ciccotti, *Soft Matter*, 2015, **11**, 3480–3491.

43 R. Villey, P.-P. Cortet, C. Creton and M. Ciccotti, *International Journal of Fracture*, 2017, **204**, 175–190.

44 P. Elzière, C. Dalle-Ferrier, C. Creton, É. Barthel and M. Ciccotti, *Soft matter*, 2017, **13**, 1624–1633.

45 P. Fourton, K. Piroird, M. Ciccotti and E. Barthel, *Glass Structures & Engineering*, 2020, **5**, 397–410.